INORGANIC CHEMISTRY FRONTIERS

RESEARCH ARTICLE

View Article Online
View Journal | View Issue

Cite this: *Inorg. Chem. Front.*, 2023, **10**, 2811

Constructing ultraviolet nonlinear optical crystals with large second harmonic generation and short absorption edges by using polar tetrahedral S_2O_3 groups†

Shixian Ke,[a,c] Huixin Fan,*[a] Chensheng Lin,[a] Ning Ye[d] and Min Luo*[a,b]

Received 27th January 2023,
Accepted 31st March 2023

DOI: 10.1039/d3qi00172e

rsc.li/frontiers-inorganic

It is generally considered difficult for traditional sulfates to exhibit strong second harmonic generation (SHG) responses and large birefringence values because SO_4 groups are nonpolar tetrahedral structures. However, by theoretical calculations, we found that polar tetrahedral S_2O_3 shows great improvements in anisotropy and second order polarizability compared to SO_4 while the wide band gap can be preserved. On this basis, a nonlinear optical (NLO) crystal $(NH_4)_2S_2O_3$ with excellent performance was synthesized. As expected, it exhibited a strong SHG response (3.3× that of KDP), suitable birefringence (0.077@546 nm) and a short absorption edge (238 nm). According to the first principles calculations, the polar tetrahedral S_2O_3 group is the main source for the SHG response of $(NH_4)_2S_2O_3$. These findings indicate that the polar S_2O_3 group is a kind of NLO functional group with superior comprehensive properties, and has great potential to develop more NLO crystals with superior comprehensive properties.

Introduction

As the core materials of all-solid-state lasers, nonlinear optical (NLO) crystals have been widely applied to laser medical treatment, modern laser micromachining, laser communication, *etc*.[1–7] In the past several decades, the exploration of UV (ultraviolet) NLO crystals with excellent comprehensive properties has always been a research hotspot in this field. Generally, a high-performance UV NLO crystal should meet the following conditions: a large second-harmonic generation (SHG) coefficient, appropriate birefringence and short UV cut-off edge. According to the anionic group theory,[8] π-conjugated anionic groups, such as NO_3, CO_3, and BO_3, are ideal functional units for UV NLO crystals.[4,5] Through lots of research studies into the π-conjugated systems, many excellent UV NLO crystals were developed including β-$Rb_2Al_2B_2O_7$,[9] $KBe_2BO_3F_2$,[10,11] $MB_5O_7F_3$ (M = Ca, Sr),[12,13] $NH_4B_4O_6F$,[14] $ABCO_3F$ (A = K, Rb; B = Mg, Ca, Sr),[15–17] and $M_2(NO_3)(OH)_3$ (M = Sr, Ba).[18,19] In recent years, non-π-conjugated tetrahedral groups, such as SO_4 and PO_4 groups, which are beneficial for enlarging the band gaps, have also attracted researchers' attention. However, since the tetrahedral groups SO_4 and PO_4 have approximately nonpolar T_d symmetry, their contributions to SHG coefficients and birefringence are limited. In fact, most reported NLO sulfates and phosphates either show small birefringence or weak SHG responses. Therefore, one of the most attractive research directions is enhancing the polarizability anisotropy or hyperpolarizability of sulfates and phosphates.

Recently, it was considered an effective strategy to design polar tetrahedral anionic groups with enlarged polarizability anisotropy and enhanced hyperpolarizability by the elemental substitution method. In 2019, Lu *et al.* first reported the optimization of birefringence with a polar tetrahedral anionic group.[46] Accordingly, SO_3F,[20,21] PO_3F[22,23] and PO_2F_2[24] groups have been successively uncovered as excellent NLO functional groups. Compared to nonpolar tetrahedral groups, these polar tetrahedral groups not only could retain the wide band gap, but also could improve the SHG effect and birefringence. Taking steps along this path, the polar S_2O_3 tetrahedral group which is obtained by replacing an oxygen atom with a sulfur atom in SO_4 could be expected to be a new NLO tetrahedral unit. The NLO-related properties of the S_2O_3 group and SO_4 group were calculated and are listed for comparison (Table 1). It is noteworthy that the hyperpolarizability (β_{ijk}) of the S_2O_3 group was more than 12 times that of SO_4 and the polarizability anisotropy of the S_2O_3 group was much superior to that of

[a]*Key Laboratory of Optoelectronic Materials Chemistry and Physics, Fujian Institute of Research on the Structure of Matter, Fuzhou, Fujian 350002, China. E-mail: lm8901@fjirsm.ac.cn, huixinfan@fjirsm.ac.cn*
[b]*Fujian Science & Technology Innovation Laboratory for Optoelectronic Information of China, Fuzhou, Fujian 350002, China*
[c]*ShanghaiTech University, Shanghai 200120, China*
[d]*Tianjin Key Laboratory of Functional Crystal Materials, Institute of Functional Crystal, Tianjin University of Technology, Tianjin 350108, China*
† Electronic supplementary information (ESI) available. See DOI: https://doi.org/10.1039/d3qi00172e

Table 1 Calculated NLO-related properties of isolated ideal S_2O_3 and SO_4 tetrahedra

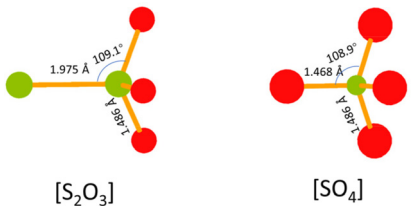

	P_x, P_y, P_z	δ	[β_{max}]	E_g (eV)
SO_4	0.00, 0.00, 0.00	45.1	47.8	6.98
S_2O_3	62.7, 62.7, 95.6	73.6	578	5.79

SO_4, indicating that the S_2O_3 group indeed has more potential for developing strong SHG and large birefringence.

In addition to strong SHG response and large birefringence, excellent UV NLO materials also require a short UV absorption edge. Although the S_2O_3 group exhibits a wide band gap, the introduction of NLO-active cations with d–d or f–f transitions would cause a significant redshift of the UV absorption edge of the material, which should be avoided. Based on these considerations, ammonium thiosulfate was discovered by screening the ICSD database[47] and is expected to be an excellent UV NLO material. First, $(NH_4)_2S_2O_3$ crystallized in the polar non-centrosymmetric (NCS) space group, *C*2, which is a basic requirement for producing SHG responses. Second, in $(NH_4)_2S_2O_3$, the polar S_2O_3 group aligned along a specific orientation is conducive to a large SHG response and birefringence. Third, the ammonium ion group without a d orbital is an ideal cation for maintaining the short absorption edge of the UV material.

Guided by the above ideas, we successfully grew $(NH_4)_2S_2O_3$ crystals by a simple solution method. The NLO properties and the relationship between the structure and the NLO properties of the crystal were also studied. It exhibited super comprehensive properties, including a strong SHG effect of 3.3× that of KDP, a suitable birefringence of 0.077@546 nm, and a short UV absorption edge of 238 nm. These results showed that $(NH_4)_2S_2O_3$ is an excellent UV NLO crystal and the polar tetrahedron S_2O_3 group is a promising group for constructing UV NLO materials.

Experimental

Regents and synthesis

Chemicals including $Na_2S_2O_3$ (0.791 g, 5 mmol, 99%, Sinopharm) and NH_4Cl (0.535 g, 10 mmol, 99%, Sinopharm) were of analytical grade and used without further purification and were purchased from commercial sources. Single crystals of $(NH_4)_2S_2O_3$ were synthesized *via* a facile water solution method. A mixture of NH_4Cl and $Na_2S_2O_3$ was dissolved in 10 mL of deionized water. This solution was stirred until it became clear. The solution was evaporated at 298 K and after several days, bulk colorless single crystals of $(NH_4)_2S_2O_3$ were obtained.

Powder X-ray diffraction

Powder X-ray diffraction measurements of $(NH_4)_2S_2O_3$ were carried out at room temperature with a Miniflex600 powder X-ray diffractometer set with Cu Kα radiation (λ = 1.5418 Å) in the range of 2θ = 5–75° and a 0.02° scan step. The experimental X-ray powder patterns of the pure sample of $(NH_4)_2S_2O_3$ agree well with the simulated X-ray powder patterns of the $(NH_4)_2S_2O_3$ single crystal models (Fig. S1†).

Single crystal X-ray diffraction

A colorless single crystal of $(NH_4)_2S_2O_3$ was selected using an optical microscope to determine its crystal structure. The diffraction data were collected by using graphite-monochromatic Mo Kα radiation (λ = 0.71073 Å) on a Rigaku Mercury CCD diffractometer at room temperature. Then the data were integrated using the CrystalClear program, and based on the multi-scan method the data were corrected for absorption and refinement.[25] The crystal structure of $(NH_4)_2S_2O_3$ was solved using the SHELXTL program in OLEX2[26] with the direct methods. Besides, the PLATON[27] program was used to check for higher symmetry elements, and none was found. The crystallographic data and structural refinement information of $(NH_4)_2S_2O_3$ are summarized in Table 2. Atomic coordinates and equivalent isotropic displacement parameters, bond lengths and angles, and anisotropic displacement parameters ($Å^2 \times 10^3$) for $(NH_4)_2S_2O_3$ are listed in Tables S1–S3.†

Table 2 Crystallographic data and structural refinement for $(NH_4)_2S_2O_3$

Formula	$(NH_4)_2S_2O_3$
Formula mass (amu)	70.07
Temperature (K)	293(2)
λ (Å)	1.34139
Crystal system	Monoclinic
Space group	*C*2
a (Å)	10.1484(7)
b (Å)	6.4862(5)
c (Å)	8.7175(7)
α (°)	90
β (°)	93.570(7)
γ (°)	90
V ($Å^3$)	572.71(8)
Z	8
ρ (calcd) (g cm^{-3})	1.625
μ (mm^{-1})	5.089
F(000)	280
θ (°)	4.421–60.581
Index range	$-13 \le h \le 13$ $-8 \le k \le 7$ $-10 \le l \le 11$
Reflections collected/unique	3357/1084
R_{int}	0.0493
Completeness to θ = 27.42° (%)	100.0
GOF on F^2	1.123
R_1/wR_2 [$F_o^2 > 2\sigma(F_o^2)$][a]	0.0432/0.1186
R_1/wR_2 (all data)	0.0442/0.1194
Absolute structure parameter	0.08(3)

[a] $R_1(F) = \sum||F_o| - |F_c||/\sum|F_o|wR_2(F_o^2) = [\sum w(F_o^2 - F_c^2)^2/\sum w(F_o^2)^2]^{1/2}$.

Energy-dispersive X-ray spectroscopy analysis

Energy dispersive X-ray spectroscopy (EDS) analyses were performed on a scanning electron microscope (FESEM, SU-8010) equipped with an energy dispersive X-ray spectroscope. The $(NH_4)_2S_2O_3$ crystals were fixed on an aluminum sample table by using carbon conductive adhesive and tested with a focused beam with 12 μA emission current and 20 kV accelerating voltage (Fig. S2†).

Thermal analysis

Thermogravimetric analysis (TGA) was performed using a NETZSCH STA449F3 simultaneous analyzer. Clean crystals of $(NH_4)_2S_2O_3$ were ground into powder, and then the powder was placed in an Al_2O_3 crucible. With an empty Al_2O_3 crucible as a reference, the sample was heated from 30 °C to 800 °C at a rate of 10 °C min^{-1} in an atmosphere of flowing N_2 (Fig. S3†).

UV-vis diffuse reflectance spectroscopy

By using $BaSO_4$ powder as the standard (100% reflectance), UV-vis-NIR diffuse reflection data were measured and recorded using a PerkinElmer Lamda-950 UV/vis/NIR spectrophotometer at room temperature in the scan range of 200–2000 nm. In accordance with the Kubelka–Munk function, the reflection value was converted to an absorption value (Fig. S4†).[28,29]

Birefringence

The birefringence of $(NH_4)_2S_2O_3$ was measured by using a Nikon ECLIPSE LV100 POL polarizing microscope equipped with a Berek Compensator and a 546 nm light source (Fig. S5†). The birefringence was calculated using the following formula:

$$\Delta R = \Delta n \times T$$

ΔR represents the optical path difference, Δn represents the birefringence, and T represents the thickness of the crystal.

Second harmonic generation

Polycrystalline SHG signals of the $(NH_4)_2S_2O_3$ samples were investigated by using the Kurtz–Perry method[30] and measured by using a Q-switched Nd:YAG solid-state laser with a fundamental wavelength of 1064 nm. Owing to the significant correlation between the SHG efficiency and the particle size of the powder, the $(NH_4)_2S_2O_3$ crystals were ground and divided into several different particle size ranges including 25–45,45–62, 62–75, 75–109, 109–150, and 150–212 μm. As a reference, the KDP crystals were also ground and sieved following the above procedures. Then they were placed in a fixed position and irradiated by using a pulsed laser (λ = 1064 nm). The outputs of second harmonic intensity from the samples and KDP were collected by using a RIGOL DS1052E 50 MHz oscilloscope.

First-principles calculations

First-principles calculations of crystal $(NH_4)_2S_2O_3$ were performed by using a CASTEP package based on density functional theory (DFT) in Material Studio software. The exchange–correlation energy was described by Perdew–Burke–Ernzerhof (PBE) in the generalized gradient approximation (GGA).[31] To model the effective interaction between atomic nuclei and valence electrons of all the elements in $(NH_4)_2S_2O_3$, the optimized norm-conserving pseudopotentials in the Kleinman–Bylander form were used.[32] The valence configurations of $(NH_4)_2S_2O_3$ including N $2s^22p^3$, H $1s^1$, S $3s^23p^4$, and O $2s^22p^4$ were observed using a relatively small basis set without compromising calculation accuracy. A high kinetic energy cut-off of 274 eV and 1 × 2 × 2 Monkhorst–Pack[33] k-point meshes were selected for the numerical integration calculation of $(NH_4)_2S_2O_3$ in the Brillouin zone. According to the transition from valence bands to conduction bands of the electron, the imaginary part of the dielectric function was calculated. Based on the Kramers–Kronig[34] transform the real part of the dielectric function was obtained and the refractive index was determined. The calculation results of SHG coefficients d_{ij} were obtained using a formula developed by Lin's group.[35]

Results and discussion

Crystal structure

Single crystals of $(NH_4)_2S_2O_3$ crystallized in the NCS space group $C2$ (no. 5) of the monoclinic crystal system. The crystal structure of $(NH_4)_2S_2O_3$ was composed of isolated NH^{4+} and $S_2O_3^{2-}$ anionic groups. Within an asymmetric unit, there were three N atoms, two S atoms and three O atoms. Every S_2O_3 group was formed by one central S^{6+} atom coordinating with three O atoms and one S^{2-} atom, in which the S–O bond lengths ranged from 1.465(2) to 1.485(3) Å and one S═S bond was 1.975(2) Å. It is clear from Fig. 1a that there are two different orientations of S_2O_3 in the structure, $S_2O_3(1)$ group and $S_2O_3(2)$ group, both of which are arranged neatly along the b-axis. Obviously, in the a-axis and c-axis, the polarity of the $S_2O_3(1)$ group and $S_2O_3(2)$ group canceled each other out, respectively. The polarity of both S_2O_3 groups in the b-axis was superimposed, which was conducive to increasing the SHG effect. Looking at the crystal structure from the ac plane (Fig. 1b), there were three kinds of ammonium ions, $NH_4(1)$, $NH_4(2)$, and $NH_4(3)$, next to the S_2O_3 groups, which were connected by hydrogen bonds, and the adjacent S_2O_3 groups were connected by hydrogen bonds of the $NH_4(1)$ group and $NH_4(3)$ group. In contrast, the $NH_4(2)$ groups were dispersed among those $[S_2O_3NH_4]_2$ structures. The $NH_4(2)$ groups were connected to the S_2O_3 groups above or below them by hydrogen bonds to form a three-dimensional structure of $(NH_4)_2S_2O_3$ (Fig. 1c).

Thermal analysis

As shown in Fig. S3,† the title compound decomposed around 170 °C, and there was only one-step decomposition of $(NH_4)_2S_2O_3$ in the range of 170–390 °C. The 99.23% (cal. 100%) weight loss can be assigned to the complete decompo-

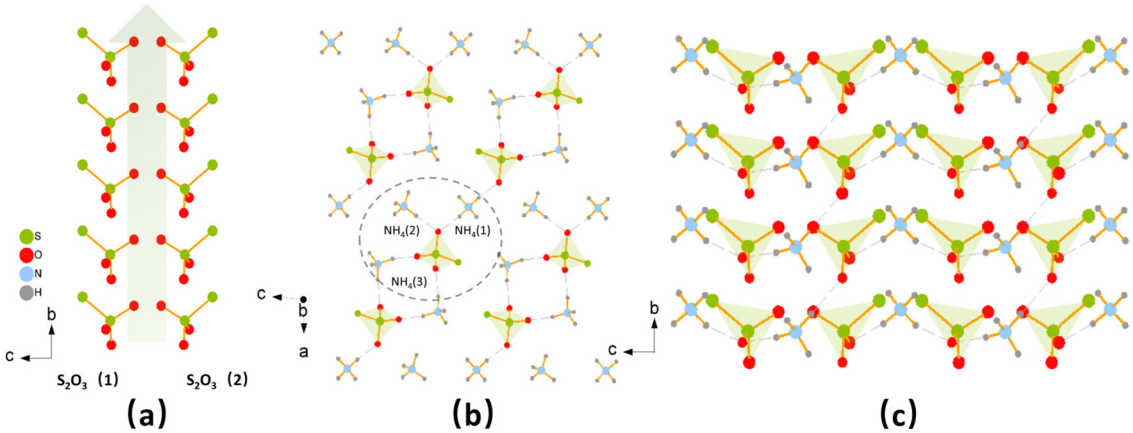

Fig. 1 (a) S_2O_3 group aligned along the *b* axis. (b) Crystal structure representations of $(NH_4)_2S_2O_3$ in the *ac* plane and (c) in the *bc* plane.

sition of $(NH_4)_2S_2O_3$ into NH_3, SO_2, S and H_2O with the evaporation of S.

UV-vis diffuse reflectance spectra

As shown in the UV-vis diffuse reflectance spectra (Fig. S4†), the absorption edge of $(NH_4)_2S_2O_3$ was down to 238 nm. According to the Kubelka–Munk function,[29] the optical band gap of $(NH_4)_2S_2O_3$ was deduced to be 4.44 eV, which was much larger than the band gap of $Na_{10}Cd(NO_3)_4(SO_3S)_4$ (E_g = 3.74 eV).[36]

Birefringence

The single crystal of $(NH_4)_2S_2O_3$ was chosen for the measurement of birefringence (Fig. S5†). The retardation value of the $(NH_4)_2S_2O_3$ crystal which was measured using a polarizing microscope (ZEISS Axio Scope A1) at a wavelength of 546 nm is 808.1 nm. Meanwhile, the thickness of the measured sample was 10.5 μm. Based on the formula $\Delta R = \Delta n \times T$, the experimental birefringence of $(NH_4)_2S_2O_3$ was 0.077 at 546 nm. The theoretical birefringence value calculated through the first-principles method ($\Delta n = |n_x - n_z|$) was 0.08 at 546 nm (Fig. 2b) which was perfectly matched with the experimental birefringence value. Compared to other NLO sulfates, such as $Rb_2Bi_2(SO_4)_2Cl_4$ (calc. 0.047 at 1064 nm),[37] $(NH_4)_2Bi_2(SO_4)_2Cl_4$ (calc. 0.055 at 1064 nm),[37] $K_2Bi_2(SO_4)_2Cl_4$ (calc. 0.056 at 1064 nm),[37] and $Nb_2O_3(IO_3)_2(SO_4)$ (calc. 0.220 at 1064 nm),[38] the birefringence of $(NH_4)_2S_2O_3$ was well suitable and could be more in line with the requirements of the phase matching ability of crystals.

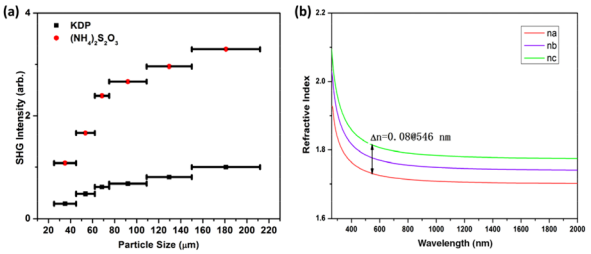

Fig. 2 (a) SHG intensity measurements of $(NH_4)_2S_2O_3$. (b) Dispersion curves of the refractive index of $(NH_4)_2S_2O_3$.

NLO properties

The powder SHG measurement was performed by the Kurtz–Perry method.[30] As shown in Fig. 2a, with KDP of the same particle size as the reference, the SHG response of $(NH_4)_2S_2O_3$ was approximately 3.3 times that of KDP at 1064 nm. As shown in Fig. 2a, the SHG responses increased when the particle sizes became larger, showing that $(NH_4)_2S_2O_3$ was phase-matchable. It is notable that the SHG effect of $(NH_4)_2S_2O_3$ was superior to those of NLO sulfates containing non-polar SO_4 groups, such as $Cs_4Mg_6(SO_4)_8$ (0.2 × KDP),[39] $Li_8NaRb_3(SO_4)_6{\cdot}2H_2O$ (0.5 × KDP),[40] $(NH_4)_2Na_3Li_9(SO_4)_7$ (0.5 × KDP),[41] $NH_4NaLi_2(SO_4)_2$ (1.1 × KDP),[41] and $Li_9Na_3Rb_2(SO_4)_7$ (1.3 × KDP).[42] The stronger SHG response of $(NH_4)_2S_2O_3$ should be due to its polar S_2O_3 groups with enhanced microscopic second order polarizability. Furthermore, as depicted in Fig. 1a, S_2O_3 was neatly arranged, which was also beneficial for improving the SHG effect of the title compound.

In order to further investigate the origin of the SHG contributions of the $(NH_4)_2S_2O_3$ crystal, the local dipole moments for the NH_4 and S_2O_3 groups were calculated. The calculated results are shown in the ESI (Table S5†). It is worth noting that the S_2O_3 polar tetrahedron has a large distortion and shows a large dipole moment of 13.67 Debye. It is even more important that in a unit cell of the title compound, the dipole moment of four S_2O_3 groups adopts a superimposed arrangement mode on the *y*-axis which results in a large dipole moment of −33.44 Debye, which is the key component for the whole dipole moment (−34.88 Debye). In polar materials, a large net dipole moment usually implies a large SHG response.[43,44] Therefore, the large SHG response of $(NH_4)_2S_2O_3$ can be attributed to the polar tetrahedron S_2O_3 groups with a large distortion and their superimposed dipole moments along the *y*-axis.

Theoretical calculations

In order to gain insight into the optical properties of $(NH_4)_2S_2O_3$, the first-principles calculations of $(NH_4)_2S_2O_3$ were carried out. The calculated band gap of $(NH_4)_2S_2O_3$ was about 4.106 eV (Fig. 3b), which was in good agreement with the experimental value of 4.44 eV. N $2s^2 2p^3$, H $1s^1$, S $3s^2 3p^4$, and O $2s^2 2p^4$ were used for calculations of the total and partial densities of states (DOS and PDOS) of $(NH_4)_2S_2O_3$ as shown in Fig. 3a. The optical properties of the compounds depended largely on the states near the forbidden band; so only the valence band (VB) top and the conduction band (CB) bottom were analyzed. It was obvious that the VBs were mostly contributed by S 3p and O 2p and the CBs were mainly due to S 3p, O 2p, N 2P, and H 1s, respectively. From the above analysis, it was clear that the optical properties of $(NH_4)_2S_2O_3$ were attributed mainly to the S_2O_3 polar tetrahedral groups.

According to the formula proposed by Lin *et al.*,[35] the SHG coefficient d_{ij} of $(NH_4)_2S_2O_3$ was calculated. $(NH_4)_2S_2O_3$ crystallized in the 2 point group. Considering the Kleinman symmetry, four independent SHG tensors including d_{21}, d_{22}, d_{23} and d_{25} of $(NH_4)_2S_2O_3$ were calculated (Fig. S7†). The largest one was d_{23} of −1.05 pm V^{-1}, which was about 2.69 times that of KDP (0.39 pm V^{-1}). It matched well with the experimental result. As shown in Fig. S6,† the occupied and unoccupied states of SHG-densities for the largest tensor d_{23} were calculated to further confirm the contributions of the S_2O_3 group to the macroscopic hyperpolarizability. In Fig. S6a,† it is obvious that the sources of SHG densities in the occupied states were mainly contributed by the S_2O_3 group. For the unoccupied states, the SHG weighted densities were mostly contributed by the S_2O_3 group and NH_4 group (Fig. S6b†). It could be concluded that the S_2O_3 groups made great contributions to the SHG response in $(NH_4)_2S_2O_3$. Atom contributions to SHG coefficients were calculated to investigate the origin of the SHG effect intuitively.[48–50] The SHG-contribution of the S_2O_3 tetrahedron to the SHG response of $(NH_4)_2S_2O_3$ was 66.9%, which was about twice as much as that of NH_4. This result further confirmed that the S_2O_3 group played a major role in the improvement of the SHG response.

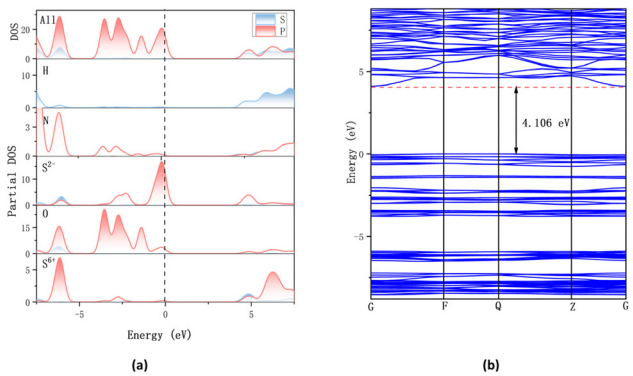

Fig. 3 (a) Total and partial DOS curves for $(NH_4)_2S_2O_3$. (b) Calculated electronic band structure for $(NH_4)_2S_2O_3$.

Conclusions

In a word, we have successfully synthesized a high-performance NLO thiosulfate $(NH_4)_2S_2O_3$ *via* a water solution method under mild conditions. It exhibited a short cut-off edge of 238 nm, a large SHG effect that is 3.3 times that of KDP and sufficient birefringence for phase-matching. According to the theoretical calculations, the S_2O_3 group shows a great improvement in polarizability anisotropy and hyperpolarizability compared to SO_4, which indicates that the polar tetrahedral S_2O_3 group is an outstanding functional group for building NLO materials. These materials containing the polar tetrahedral S_2O_3 group might show great improvements in the SHG effect while retaining a short UV absorption edge. It is clear that the S_2O_3 group has great potential for the synthesis of high performance nonlinear optical crystals.

Conflicts of interest

There are no conflicts to declare.

Acknowledgements

This work was supported by the National Natural Science Foundation of China (Grant No. 22222510, 21975255 and 21921001), the Foundation of Fujian Science & Technology Innovation Laboratory (2021ZR202) and the Youth Innovation Promotion Association CAS (2019303).

References

1 P. Becker, Borate materials in nonlinear optics, *Adv. Mater.*, 1998, **10**, 979.
2 Y. N. Xia, C. T. Chen, D. Y. Tang and B. C. Wu, New nonlinear optical crystals for UV and VUV harmonic generation, *Adv. Mater.*, 1995, **7**, 79.
3 G. H. Zou, C. S. Lin, H. Jo, G. Nam, T. S. You and K. M. Ok, Pb_2BO_3Cl: A Tailor-Made Polar Lead Borate Chloride with Very Strong Second Harmonic Generation, *Angew. Chem., Int. Ed.*, 2016, **55**, 12078–12082.
4 X. L. Wang, L. K. Chen, W. Li, H. L. Huang, C. Liu, C. Chen, Y. H. Luo, Z. E. Su, D. Wu, Z. D. Li, H. Lu, Y. Hu, X. Jiang, C. Z. Peng, L. Li, N. L. Liu, Y. A. Chen, C. Y. Lu and J. W. Pan, Experimental Ten-Photon Entanglement, *Phys. Rev. Lett.*, 2016, **117**, 210502.
5 H. Tian, C. S. Lin and X. Zhao, Design of a new ultraviolet nonlinear optical material $KNO_3SO_3NH_3$ exhibiting an unexpected strong second harmonic generation response, *Mater. Today Phys.*, 2022, **28**, 100849.
6 X. Dong, L. Huang, C. Hu, H. Zeng, Z. Lin, X. Wang, K. M. Ok and G. Zou, $CsSbF_2SO_4$: An Excellent Ultraviolet Nonlinear Optical Sulfate with a KTiOPO4 (KTP)-type Structure, *Angew. Chem., Int. Ed.*, 2019, **58**, 6528–6534.

7 H. Tian, C. S. Lin, X. Zhao, F. Xu, C. Wang, N. Ye and M. Luo, $Ba(SO_3CH_3)_2$: a Deep-Ultraviolet Transparent Crystal with Excellent Optical Nonlinearity Based on a New Polar Non-π-conjugated NLO Building Unit $SO_3CH_3^-$, *CCS Chem.*, 2023, DOI: 10.31635/ccschem.022.202202582.
8 C. T. Chen, A Localized Quantal Theoretical Treatment Based on an Anionic Coordination Polyhedron Model for the EO and SHG Effects in Crystals of the Mixed-Oxided Types, *Sci. Sin.*, 1979, **22**, 756–776.
9 T. T. Tran, N. Z. Koocher, J. M. Rondinelli and P. S. Halasyamani, Beryllium-Free β-$Rb_2Al_2B_2O_7$ as a Possible Deep-Ultraviolet Nonlinear Optical Material Replacement for $KBe_2BO_3F_2$, *Angew. Chem., Int. Ed.*, 2017, **56**, 2969–2973.
10 B. C. Wu, D. Y. Tang, N. Ye and C. T. Chen, Linear and nonlinear optical properties of the $KBe_2BO_3F_2$ (KBBF) crystal, *Opt. Mater.*, 1996, **5**, 105–109.
11 C. T. Chen, Z. Y. Xu, D. Q. Deng, J. Zhang, G. K. L. Wong, B. C. Wu, N. Ye and D. Y. Tang, The vacuum ultraviolet phase-matching characteristics of nonlinear optical $KBe_2BO_3F_2$ crystal, *Appl. Phys. Lett.*, 1996, **68**, 2930–2932.
12 Z. Z. Zhang, Y. Wang, B. B. Zhang, Z. H. Yang and S. L. Pan, $CaB_5O_7F_3$: A Beryllium-Free Alkaline-Earth Fluorooxoborate Exhibiting Excellent Nonlinear Optical Performances, *Inorg. Chem.*, 2018, **57**, 4820–4823.
13 M. Mutailipu, M. Zhang, B. B. Zhang, L. Y. Wang, Z. L. Yang, X. Zhou and S. L. Pan, $SrB_5O_7F_3$ Functionalized with $[B_5O_9F_3]_6^-$ Chromophores: Accelerating the Rational Design of Deep-Ultraviolet Nonlinear Optical Materials, *Angew. Chem., Int. Ed.*, 2018, **57**, 6095–6099.
14 G. Q. Shi, Y. Wang, F. F. Zhang, B. B. Zhang, Z. H. Yang, X. L. Hou, S. L. Pan and K. R. Poeppelmeier, Finding the Next Deep-Ultraviolet Nonlinear Optical Material: $NH_4B_4O_6F$, *J. Am. Chem. Soc.*, 2017, **139**, 10645–10648.
15 T. T. Tran, J. Young, J. M. Rondinelli and P. S. Halasyamani, Mixed-Metal Carbonate Fluorides as Deep-Ultraviolet Nonlinear Optical Materials, *J. Am. Chem. Soc.*, 2017, **139**, 1285–1295.
16 T. T. Tran, J. G. He, J. M. Rondinelli and P. S. Halasyamani, $RbMgCO_3F$: A New Beryllium-Free Deep-Ultraviolet Nonlinear Optical Material, *J. Am. Chem. Soc.*, 2015, **137**, 10504–10507.
17 G. H. Zou, N. Ye, L. Huang and X. S. Lin, Alkaline-Alkaline Earth Fluoride Carbonate Crystals $ABCO_3F$ (A = K, Rb, Cs; B = Ca, Sr, Ba) as Nonlinear Optical Materials, *J. Am. Chem. Soc.*, 2011, **133**, 20001–20007.
18 L. Huang, G. H. Zou, H. Q. Cai, S. C. Wang, C. S. Lin and N. Ye, $Sr_2(OH)_3NO_3$: the first nitrate as a deep UV nonlinear optical material with large SHG responses, *J. Mater. Chem. C*, 2015, **3**, 5268–5274.
19 X. H. Dong, L. Huang, Q. Y. Liu, H. M. Zeng, Z. E. Lin, D. G. Xu and G. H. Zou, Perfect balance harmony in $Ba_2NO_3(OH)_3$: a beryllium-free nitrate as a UV nonlinear optical material, *Chem. Commun.*, 2018, **54**, 5792–5795.
20 M. Luo, C. Lin, D. Lin and N. Ye, Rational Design of the Metal-Free $KBe_2BO_3F_2$ (KBBF) Family Member $C(NH_2)_3SO_3F$ with Ultraviolet Optical Nonlinearity, *Angew. Chem., Int. Ed.*, 2020, **37**, 15978–15981.
21 Y. Sun, C. Lin and S. F, $K_2(BeS)O_4F_2$: a novel fluorosulfate with unprecedented 1D $[(BeO_3F)\text{-}(SO_3F)]_\infty$ chains exhibiting large birefringence, *Inorg. Chem. Front.*, 2022, **9**, 6490–6497.
22 B. B. Zhang, G. Q. Shi, Z. H. Yang, F. F. Zhang and S. L. Pan, Fluorooxoborates: Beryllium-Free Deep-Ultraviolet Nonlinear Optical Materials without Layered Growth, *Angew. Chem., Int. Ed.*, 2017, **56**, 3916–3919.
23 L. Xiong, J. Chen, J. Lu, C. Y. Pan and L. M. Wu, Monofluorophosphates: A New Source of Deep-Ultraviolet Nonlinear Optical Materials, *Chem. Mater.*, 2018, **30**, 7823–7830.
24 B. B. Zhang, G. P. Han, Y. Wang, X. L. Chen, Z. H. Yang and S. L. Pan, Expanding Frontiers of Ultraviolet Nonlinear Optical Materials with Fluorophosphates, *Chem. Mater.*, 2018, **30**, 5397–5403.
25 R. H. Blessing, An Empirical Correction for Absorption Anisotropy, *Acta Crystallogr., Sect. A: Found. Adv.*, 1995, **51**, 33–38.
26 O. V. Dolomanov, L. J. Bourhis, R. J. Gildea, J. A. K. Howard and H. Puschmann, OLEX2: a complete structure solution, refinement and analysis program, *J. Appl. Crystallogr.*, 2009, **42**, 339–341.
27 A. L. Spek, Single-crystal structure validation with the program PLATON, *J. Appl. Crystallogr.*, 2003, **36**, 7–13.
28 J. Tauc, Absorption Edge and Internal Electric Fields in Amorphous Semiconductors, *Mater. Res. Bull.*, 1970, **5**, 721–729.
29 P. Kubelka and F. Munk, An article on optics of paint layers, *Z. Tech. Phys.*, 1931, **12**(1), 886–892.
30 S. K. Kurtz and T. T. Perry, A Powder Technique for Evaluation of Nonlinear Optical Materials, *J. Appl. Phys.*, 1968, **39**, 3798–3813.
31 J. P. Perdew, A. Ruzsinszky, G. I. Csonka, O. A. Vydrov, G. E. Scuseria, L. A. Constantin, X. Zhou and K. Burke, Restoring the Density-Gradient Expansion for Exchange in Solids and Surfaces, *Phys. Rev. Lett.*, 2008, **100**, 136406.
32 A. M. Rappe, K. M. Rabe, E. Kaxiras and J. D. Joannopoulos, Optimized Pseudopotentials, *Phys. Rev. B: Condens. Matter Mater. Phys.*, 1990, **41**, 1227–1230.
33 H. J. Monkhorst and J. D. Pack, Special Points for Brillouin-Zone Integrations, *Phys. Rev. B: Solid State*, 1976, **13**, 5188–5192.
34 E. D. Palik, Handbook of Optical Constants of Solids, *Academic Press*, 1985.
35 J. Lin, M. H. Lee, Z. P. Liu, C. T. Chen and C. J. Pickard, Mechanism for linear and nonlinear optical effects in β-BaB_2O_4 crystals, *Phys. Rev. B: Condens. Matter Mater. Phys.*, 1999, **60**, 13380–13389; Z. S. Lin, X. X. Jiang, L. Kang, P. F. Gong, S. Y. Luo and M. H. Lee, Theoretical calculations and predictions of the nonlinear optical coefficients of borate crystals, *J. Phys. D: Appl. Phys.*, 2014, **47**, 253001.
36 Y. Liu, Y. Liu, Z. Lin, Y. Li, Q. Ding, X. Chen, L. Li, S. Zhao, M. Hong and J. Luo, Nonpolar $Na_{10}Cd(NO_3)_4(SO_3S)_4$

Exhibits a Large Second-Harmonic Generation, *CCS Chem.*, 2021, **4**, 526–531.

37 K. C. Chen, Y. Yang, G. Peng, S. D. Yang, T. Yan, H. X. Fan, Z. S. Lin and N. Ye, $A_2Bi_2(SO_4)_2Cl_4$ (A = NH_4, K, Rb): achieving a subtle balance of the large second harmonic generation effect and sufficient birefringence in sulfate nonlinear optical materials, *J. Mater. Chem. C*, 2019, **7**, 9900–9907.

38 H. X. Tang, Y. X. Zhang, C. Zhuo, R. B. Fu, H. Lin, Z. J. Ma and X. T. Wu, A Niobium Oxyiodate Sulfate with a Strong Second Harmonic-Generation Response Built by Rational Multi-Component Design, *Angew. Chem., Int. Ed.*, 2019, **58**, 3824–3828.

39 Y. Q. Li, J. H. Luo, X. H. Ji and S. G. Zhao, A Short-wave UV Nonlinear Optical Sulfate of High Thermal Stability, *Chin. J. Struct. Chem.*, 2020, **39**(3), 485–492.

40 Y. Q. Li, S. E. Zhao, P. Shan, X. F. Li, Q. R. Ding, S. Liu, Z. Y. Wu, S. S. Wang, L. N. Li and J. H. Luo, $Li_8NaRb_3(SO_4)_6{\cdot}2H_2O$ as a new sulfate deep-ultraviolet nonlinear optical material, *J. Mater. Chem. C*, 2018, **6**, 12240–12244.

41 Y. Q. Li, F. Liang, S. G. Zhao, L. N. Li, Z. Y. Wu, Q. R. Ding, S. Liu, Z. S. Lin, M. C. Hong and J. H. Luo, Two Non-π-Conjugated Deep-UV Nonlinear Optical Sulfates, *J. Am. Chem. Soc.*, 2019, **141**, 3833–3837.

42 Y. Li, C. Yin, X. Yang, X. Kuang, J. Chen, L. He, Q. Ding, S. Zhao, M. Hong and J. Luo, Nonlinear Optical Switchable Sulfate of Ultrawide Bandgap, *CCS Chem.*, 2021, **3**, 2298–2306.

43 H. Yu, H. Wu, S. Pan, Z. Yang, X. Hou, X. Su, Q. Jing, K. R. Poeppelmeier and J. M. Rondinelli, $Cs_3Zn_6B_9O_{21}$: A Chemically Benign Member of the KBBF Family Exhibiting the Largest Second Harmonic Generation Response, *J. Am. Chem. Soc.*, 2014, **136**, 1264.

44 H. Wu, S. Pan, K. R. Poeppelmeier, H. Li, D. Jia, Z. Chen, X. Fan, Y. Yang, J. M. Rondinelli and H. Luo, $K_3B_6O_{10}Cl$: A New Structure Analogous to Perovskite with a Large Second Harmonic Generation Response and Deep UV Absorption Edge, *J. Am. Chem. Soc.*, 2011, **133**, 7786.

45 M. Mutailipu, K. R. Poeppelmeier and S. Pan, Borates: A Rich Source for Optical Materials, *Chem. Rev.*, 2021, **121**(3), 1130–1202.

46 J. Lu, J. Yue, L. Xiong, W. Zhang, L. Chen and L. Wu, Uniform Alignment of Non-π-Conjugated Species Enhances Deep Ultraviolet Optical Nonlinearity, *J. Am. Chem. Soc.*, 2019, **141**, 8093–8097.

47 S. T. Teng, H. Fuess and J. W. Bats, Ammonium thiosulphate, *Acta Crystallogr., Sect. B: Struct. Crystallogr. Cryst. Chem.*, 1979, **35**, 1682–1684.

48 J. E. Sipe and E. Ghahramani, Nonlinear-Optical Response Of Semiconductors In The Independent-Particle Approximation, *Phys. Rev. B: Condens. Matter Mater. Phys.*, 1993, **48**, 11705–11722.

49 A. Zhou, C. Lin, B. Li, W. Cheng, Z. Guo, Z. Hou, F. Yuan and G. Chai, $Ba_6In_6Zn_4Se_{19}$: A High Performance Infrared Nonlinear Optical Crystal with $[InSe_3]^{3-}$ Trigonal Planar Functional Motifs, *J. Mater. Chem. C*, 2020, **8**(23), 7947–7955.

50 C. Lin, A. Zhou, W. Cheng, N. Ye and G. Chai, Atom-Resolved Analysis of Birefringence of Nonlinear Optical Crystals by Bader Charge Integration, *J. Phys. Chem. C*, 2019, **123**, 31183–31189.